Measurement of the branching fraction and Lamda[over-bar] polarization in B0-->Lambda[over-bar]pPi[superscript -]

Measurement of the branching fraction and $\bar{\Lambda}$ polarization in $B^0 \to \bar{\Lambda} p \pi^-$

B. Aubert,[1] Y. Karyotakis,[1] J. P. Lees,[1] V. Poireau,[1] E. Prencipe,[1] X. Prudent,[1] V. Tisserand,[1] J. Garra Tico,[2] E. Grauges,[2] M. Martinelli,[3a,3b] A. Palano,[3a,3b] M. Pappagallo,[3a,3b] G. Eigen,[4] B. Stugu,[4] L. Sun,[4] M. Battaglia,[5] D. N. Brown,[5] L. T. Kerth,[5] Yu. G. Kolomensky,[5] G. Lynch,[5] I. L. Osipenkov,[5] K. Tackmann,[5] T. Tanabe,[5] C. M. Hawkes,[6] N. Soni,[6] A. T. Watson,[6] H. Koch,[7] T. Schroeder,[7] D. J. Asgeirsson,[8] B. G. Fulsom,[8] C. Hearty,[8] T. S. Mattison,[8] J. A. McKenna,[8] M. Barrett,[9] A. Khan,[9] A. Randle-Conde,[9] V. E. Blinov,[10] A. D. Bukin,[10] A. R. Buzykaev,[10] V. P. Druzhinin,[10] V. B. Golubev,[10] A. P. Onuchin,[10] S. I. Serednyakov,[10] Yu. I. Skovpen,[10] E. P. Solodov,[10] K. Yu. Todyshev,[10] M. Bondioli,[11] S. Curry,[11] I. Eschrich,[11] D. Kirkby,[11] A. J. Lankford,[11] P. Lund,[11] M. Mandelkern,[11] E. C. Martin,[11] J. Schultz,[11] D. P. Stoker,[11] H. Atmacan,[12] J. W. Gary,[12] F. Liu,[12] O. Long,[12] G. M. Vitug,[12] Z. Yasin,[12] L. Zhang,[12] V. Sharma,[13] C. Campagnari,[14] T. M. Hong,[14] D. Kovalskyi,[14] M. A. Mazur,[14] J. D. Richman,[14] T. W. Beck,[15] A. M. Eisner,[15] C. A. Heusch,[15] J. Kroseberg,[15] W. S. Lockman,[15] A. J. Martinez,[15] T. Schalk,[15] B. A. Schumm,[15] A. Seiden,[15] L. Wang,[15] L. O. Winstrom,[15] C. H. Cheng,[16] D. A. Doll,[16] B. Echenard,[16] F. Fang,[16] D. G. Hitlin,[16] I. Narsky,[16] T. Piatenko,[16] F. C. Porter,[16] R. Andreassen,[17] G. Mancinelli,[17] B. T. Meadows,[17] K. Mishra,[17] M. D. Sokoloff,[17] P. C. Bloom,[18] W. T. Ford,[18] A. Gaz,[18] J. F. Hirschauer,[18] M. Nagel,[18] U. Nauenberg,[18] J. G. Smith,[18] S. R. Wagner,[18] R. Ayad,[19,†] W. H. Toki,[19] R. J. Wilson,[19] E. Feltresi,[20] A. Hauke,[20] H. Jasper,[20] T. M. Karbach,[20] J. Merkel,[20] A. Petzold,[20] B. Spaan,[20] K. Wacker,[20] M. J. Kobel,[21] R. Nogowski,[21] K. R. Schubert,[21] R. Schwierz,[21] A. Volk,[21] D. Bernard,[22] E. Latour,[22] M. Verderi,[22] P. J. Clark,[23] S. Playfer,[23] J. E. Watson,[23] M. Andreotti,[24a,24b] D. Bettoni,[24a] C. Bozzi,[24a] R. Calabrese,[24a,24b] A. Cecchi,[24a,24b] G. Cibinetto,[24a,24b] E. Fioravanti,[24a,24b] P. Franchini,[24a,24b] E. Luppi,[24a,24b] M. Munerato,[24a,24b] M. Negrini,[24a,24b] A. Petrella,[24a,24b] L. Piemontese,[24a] V. Santoro,[24a,24b] R. Baldini-Ferroli,[25] A. Calcaterra,[25] R. de Sangro,[25] G. Finocchiaro,[25] S. Pacetti,[25] P. Patteri,[25] I. M. Peruzzi,[25,‡] M. Piccolo,[25] M. Rama,[25] A. Zallo,[25] R. Contri,[26a,26b] E. Guido,[26a,26b] M. Lo Vetere,[26a,26b] M. R. Monge,[26a,26b] S. Passaggio,[26a] C. Patrignani,[26a,26b] E. Robutti,[26a] S. Tosi,[26a,26b] K. S. Chaisanguanthum,[27] M. Morii,[27] A. Adametz,[28] J. Marks,[28] S. Schenk,[28] U. Uwer,[28] F. U. Bernlochner,[29] V. Klose,[29] H. M. Lacker,[29] D. J. Bard,[30] P. D. Dauncey,[30] M. Tibbetts,[30] P. K. Behera,[31] M. J. Charles,[31] U. Mallik,[31] J. Cochran,[32] H. B. Crawley,[32] L. Dong,[32] V. Eyges,[32] W. T. Meyer,[32] S. Prell,[32] E. I. Rosenberg,[32] A. E. Rubin,[32] Y. Y. Gao,[33] A. V. Gritsan,[33] Z. J. Guo,[33] N. Arnaud,[34] J. Béquilleux,[34] A. D'Orazio,[34] M. Davier,[34] D. Derkach,[34] J. Firmino da Costa,[34] G. Grosdidier,[34] F. Le Diberder,[34] V. Lepeltier,[34] A. M. Lutz,[34] B. Malaescu,[34] S. Pruvot,[34] P. Roudeau,[34] M. H. Schune,[34] J. Serrano,[34] V. Sordini,[34,§] A. Stocchi,[34] G. Wormser,[34] D. J. Lange,[35] D. M. Wright,[35] I. Bingham,[36] J. P. Burke,[36] C. A. Chavez,[36] J. R. Fry,[36] E. Gabathuler,[36] R. Gamet,[36] D. E. Hutchcroft,[36] D. J. Payne,[36] C. Touramanis,[36] A. J. Bevan,[37] C. K. Clarke,[37] F. Di Lodovico,[37] R. Sacco,[37] M. Sigamani,[37] G. Cowan,[38] S. Paramesvaran,[38] A. C. Wren,[38] D. N. Brown,[39] C. L. Davis,[39] A. G. Denig,[40] M. Fritsch,[40] W. Gradl,[40] A. Hafner,[40] K. E. Alwyn,[41] D. Bailey,[41] R. J. Barlow,[41] G. Jackson,[41] G. D. Lafferty,[41] T. J. West,[41] J. I. Yi,[41] J. Anderson,[42] C. Chen,[42] A. Jawahery,[42] D. A. Roberts,[42] G. Simi,[42] J. M. Tuggle,[42] C. Dallapiccola,[43] E. Salvati,[43] S. Saremi,[43] R. Cowan,[44] D. Dujmic,[44] P. H. Fisher,[44] S. W. Henderson,[44] G. Sciolla,[44] M. Spitznagel,[44] R. K. Yamamoto,[44] M. Zhao,[44] P. M. Patel,[45] S. H. Robertson,[45] M. Schram,[45] A. Lazzaro,[46a,46b] V. Lombardo,[46a] F. Palombo,[46a,46b] S. Stracka,[46a,46b] J. M. Bauer,[47] L. Cremaldi,[47] R. Godang,[47,‖] R. Kroeger,[47] P. Sonnek,[47] D. J. Summers,[47] H. W. Zhao,[47] M. Simard,[48] P. Taras,[48] H. Nicholson,[49] G. De Nardo,[50a,50b] L. Lista,[50a] D. Monorchio,[50a,50b] G. Onorato,[50a,50b] C. Sciacca,[50a,50b] G. Raven,[51] H. L. Snoek,[51] C. P. Jessop,[52] K. J. Knoepfel,[52] J. M. LoSecco,[52] W. F. Wang,[52] L. A. Corwin,[53] K. Honscheid,[53] H. Kagan,[53] R. Kass,[53] J. P. Morris,[53] A. M. Rahimi,[53] J. J. Regensburger,[53] S. J. Sekula,[53] Q. K. Wong,[53] N. L. Blount,[54] J. Brau,[54] R. Frey,[54] O. Igonkina,[54] J. A. Kolb,[54] M. Lu,[54] R. Rahmat,[54] N. B. Sinev,[54] D. Strom,[54] J. Strube,[54] E. Torrence,[54] G. Castelli,[55a,55b] N. Gagliardi,[55a,55b] M. Margoni,[55a,55b] M. Morandin,[55a] M. Posocco,[55a] M. Rotondo,[55a] F. Simonetto,[55a,55b] R. Stroili,[55a,55b] C. Voci,[55a,55b] P. del Amo Sanchez,[56] E. Ben-Haim,[56] G. R. Bonneaud,[56] H. Briand,[56] J. Chauveau,[56] O. Hamon,[56] Ph. Leruste,[56] G. Marchiori,[56] J. Ocariz,[56] A. Perez,[56] J. Prendki,[56] S. Sitt,[56] L. Gladney,[57] M. Biasini,[58a,58b] E. Manoni,[58a,58b] C. Angelini,[59a,59b] G. Batignani,[59a,59b] S. Bettarini,[59a,59b] G. Calderini,[59a,59b,¶] M. Carpinelli,[59a,59b,**] A. Cervelli,[59a,59b] F. Forti,[59a,59b] M. A. Giorgi,[59a,59b] A. Lusiani,[59a,59c] M. Morganti,[59a,59b] N. Neri,[59a,59b] E. Paoloni,[59a,59b] G. Rizzo,[59a,59b] J. J. Walsh,[59a] D. Lopes Pegna,[60] C. Lu,[60] J. Olsen,[60] A. J. S. Smith,[60] A. V. Telnov,[60] F. Anulli,[61a] E. Baracchini,[61a,61b] G. Cavoto,[61a] R. Faccini,[61a,61b] F. Ferrarotto,[61a] F. Ferroni,[61a,61b] M. Gaspero,[61a,61b] P. D. Jackson,[61a] L. Li Gioi,[61a] M. A. Mazzoni,[61a] S. Morganti,[61a] G. Piredda,[61a] F. Renga,[61a,61b] C. Voena,[61a] M. Ebert,[62] T. Hartmann,[62] H. Schröder,[62] R. Waldi,[62] T. Adye,[63] B. Franek,[63] E. O. Olaiya,[63] F. F. Wilson,[63] S. Emery,[64] L. Esteve,[64] G. Hamel de Monchenault,[64] W. Kozanecki,[64] G. Vasseur,[64] Ch. Yèche,[64] M. Zito,[64] M. T. Allen,[65] D. Aston,[65] R. Bartoldus,[65] J. F. Benitez,[65] R. Cenci,[65] J. P. Coleman,[65]

M. R. Convery,[65] J. C. Dingfelder,[65] J. Dorfan,[65] G. P. Dubois-Felsmann,[65] W. Dunwoodie,[65] R. C. Field,[65] M. Franco Sevilla,[65] A. M. Gabareen,[65] M. T. Graham,[65] P. Grenier,[65] C. Hast,[65] W. R. Innes,[65] J. Kaminski,[65] M. H. Kelsey,[65] H. Kim,[65] P. Kim,[65] M. L. Kocian,[65] D. W. G. S. Leith,[65] S. Li,[65] B. Lindquist,[65] S. Luitz,[65] V. Luth,[65] H. L. Lynch,[65] D. B. MacFarlane,[65] H. Marsiske,[65] R. Messner,[65,*] D. R. Muller,[65] H. Neal,[65] S. Nelson,[65] C. P. O'Grady,[65] I. Ofte,[65] M. Perl,[65] B. N. Ratcliff,[65] A. Roodman,[65] A. A. Salnikov,[65] R. H. Schindler,[65] J. Schwiening,[65] A. Snyder,[65] D. Su,[65] M. K. Sullivan,[65] K. Suzuki,[65] S. K. Swain,[65] J. M. Thompson,[65] J. Va'vra,[65] A. P. Wagner,[65] M. Weaver,[65] C. A. West,[65] W. J. Wisniewski,[65] M. Wittgen,[65] D. H. Wright,[65] H. W. Wulsin,[65] A. K. Yarritu,[65] C. C. Young,[65] V. Ziegler,[65] X. R. Chen,[66] H. Liu,[66] W. Park,[66] M. V. Purohit,[66] R. M. White,[66] J. R. Wilson,[66] P. R. Burchat,[67] A. J. Edwards,[67] T. S. Miyashita,[67] S. Ahmed,[68] M. S. Alam,[68] J. A. Ernst,[68] B. Pan,[68] M. A. Saeed,[68] S. B. Zain,[68] A. Soffer,[69] S. M. Spanier,[70] B. J. Wogsland,[70] R. Eckmann,[71] J. L. Ritchie,[71] A. M. Ruland,[71] C. J. Schilling,[71] R. F. Schwitters,[71] B. C. Wray,[71] B. W. Drummond,[72] J. M. Izen,[72] X. C. Lou,[72] F. Bianchi,[73a,73b] D. Gamba,[73a,73b] M. Pelliccioni,[73a,73b] M. Bomben,[74a,74b] L. Bosisio,[74a,74b] C. Cartaro,[74a,74b] G. Della Ricca,[74a,74b] L. Lanceri,[74a,74b] L. Vitale,[74a,74b] V. Azzolini,[75] N. Lopez-March,[75] F. Martinez-Vidal,[75] D. A. Milanes,[75] A. Oyanguren,[75] J. Albert,[76] Sw. Banerjee,[76] B. Bhuyan,[76] H. H. F. Choi,[76] K. Hamano,[76] G. J. King,[76] R. Kowalewski,[76] M. J. Lewczuk,[76] I. M. Nugent,[76] J. M. Roney,[76] R. J. Sobie,[76] T. J. Gershon,[77] P. F. Harrison,[77] J. Ilic,[77] T. E. Latham,[77] G. B. Mohanty,[77] E. M. T. Puccio,[77] H. R. Band,[78] X. Chen,[78] S. Dasu,[78] K. T. Flood,[78] Y. Pan,[78] R. Prepost,[78] C. O. Vuosalo,[78] and S. L. Wu[78]

(*BABAR* Collaboration)

[1]*Laboratoire d'Annecy-le-Vieux de Physique des Particules (LAPP), Université de Savoie, CNRS/IN2P3, F-74941 Annecy-Le-Vieux, France*
[2]*Universitat de Barcelona, Facultat de Fisica, Departament ECM, E-08028 Barcelona, Spain*
[3a]*INFN Sezione di Bari, I-70126 Bari, Italy*
[3b]*Dipartimento di Fisica, Università di Bari, I-70126 Bari, Italy*
[4]*University of Bergen, Institute of Physics, N-5007 Bergen, Norway*
[5]*Lawrence Berkeley National Laboratory and University of California, Berkeley, California 94720, USA*
[6]*University of Birmingham, Birmingham, B15 2TT, United Kingdom*
[7]*Ruhr Universität Bochum, Institut für Experimentalphysik 1, D-44780 Bochum, Germany*
[8]*University of British Columbia, Vancouver, British Columbia, Canada V6T 1Z1*
[9]*Brunel University, Uxbridge, Middlesex UB8 3PH, United Kingdom*
[10]*Budker Institute of Nuclear Physics, Novosibirsk 630090, Russia*
[11]*University of California at Irvine, Irvine, California 92697, USA*
[12]*University of California at Riverside, Riverside, California 92521, USA*
[13]*University of California at San Diego, La Jolla, California 92093, USA*
[14]*University of California at Santa Barbara, Santa Barbara, California 93106, USA*
[15]*University of California at Santa Cruz, Institute for Particle Physics, Santa Cruz, California 95064, USA*
[16]*California Institute of Technology, Pasadena, California 91125, USA*
[17]*University of Cincinnati, Cincinnati, Ohio 45221, USA*
[18]*University of Colorado, Boulder, Colorado 80309, USA*
[19]*Colorado State University, Fort Collins, Colorado 80523, USA*
[20]*Technische Universität Dortmund, Fakultät Physik, D-44221 Dortmund, Germany*
[21]*Technische Universität Dresden, Institut für Kernund Teilchenphysik, D-01062 Dresden, Germany*
[22]*Laboratoire Leprince-Ringuet, CNRS/IN2P3, Ecole Polytechnique, F-91128 Palaiseau, France*
[23]*University of Edinburgh, Edinburgh EH9 3JZ, United Kingdom*
[24a]*INFN Sezione di Ferrara, I-44100 Ferrara, Italy*
[24b]*Dipartimento di Fisica, Università di Ferrara, I-44100 Ferrara, Italy*
[25]*INFN Laboratori Nazionali di Frascati, I-00044 Frascati, Italy*
[26a]*INFN Sezione di Genova, I-16146 Genova, Italy*
[26b]*Dipartimento di Fisica, Università di Genova, I-16146 Genova, Italy*
[27]*Harvard University, Cambridge, Massachusetts 02138, USA*
[28]*Universität Heidelberg, Physikalisches Institut, Philosophenweg 12, D-69120 Heidelberg, Germany*
[29]*Humboldt-Universität zu Berlin, Institut für Physik, Newtonstr. 15, D-12489 Berlin, Germany*
[30]*Imperial College London, London, SW7 2AZ, United Kingdom*
[31]*University of Iowa, Iowa City, Iowa 52242, USA*
[32]*Iowa State University, Ames, Iowa 50011-3160, USA*
[33]*Johns Hopkins University, Baltimore, Maryland 21218, USA*

[34]Laboratoire de l'Accélérateur Linéaire, IN2P3/CNRS et Université Paris-Sud 11, Centre Scientifique d'Orsay, B. P. 34, F-91898 Orsay Cedex, France
[35]Lawrence Livermore National Laboratory, Livermore, California 94550, USA
[36]University of Liverpool, Liverpool L69 7ZE, United Kingdom
[37]Queen Mary, University of London, London, E1 4NS, United Kingdom
[38]University of London, Royal Holloway and Bedford New College, Egham, Surrey TW20 0EX, United Kingdom
[39]University of Louisville, Louisville, Kentucky 40292, USA
[40]Johannes Gutenberg-Universität Mainz, Institut für Kernphysik, D-55099 Mainz, Germany
[41]University of Manchester, Manchester M13 9PL, United Kingdom
[42]University of Maryland, College Park, Maryland 20742, USA
[43]University of Massachusetts, Amherst, Massachusetts 01003, USA
[44]Massachusetts Institute of Technology, Laboratory for Nuclear Science, Cambridge, Massachusetts 02139, USA
[45]McGill University, Montréal, Québec, Canada H3A 2T8
[46a]INFN Sezione di Milano, I-20133 Milano, Italy
[46b]Dipartimento di Fisica, Università di Milano, I-20133 Milano, Italy
[47]University of Mississippi, University, Mississippi 38677, USA
[48]Université de Montréal, Physique des Particules, Montréal, Québec, Canada H3C 3J7
[49]Mount Holyoke College, South Hadley, Massachusetts 01075, USA
[50a]INFN Sezione di Napoli, I-80126 Napoli, Italy
[50b]Dipartimento di Scienze Fisiche, Università di Napoli Federico II, I-80126 Napoli, Italy
[51]NIKHEF, National Institute for Nuclear Physics and High Energy Physics, NL-1009 DB Amsterdam, The Netherlands
[52]University of Notre Dame, Notre Dame, Indiana 46556, USA
[53]Ohio State University, Columbus, Ohio 43210, USA
[54]University of Oregon, Eugene, Oregon 97403, USA
[55a]INFN Sezione di Padova, I-35131 Padova, Italy
[55b]Dipartimento di Fisica, Università di Padova, I-35131 Padova, Italy
[56]Laboratoire de Physique Nucléaire et de Hautes Energies, IN2P3/CNRS, Université Pierre et Marie Curie-Paris6, Université Denis Diderot-Paris7, F-75252 Paris, France
[57]University of Pennsylvania, Philadelphia, Pennsylvania 19104, USA
[58a]INFN Sezione di Perugia, I-06100 Perugia, Italy
[58b]Dipartimento di Fisica, Università di Perugia, I-06100 Perugia, Italy
[59a]INFN Sezione di Pisa, I-56127 Pisa, Italy
[59b]Dipartimento di Fisica, Università di Pisa, I-56127 Pisa, Italy
[59c]Scuola Normale Superiore di Pisa, I-56127 Pisa, Italy
[60]Princeton University, Princeton, New Jersey 08544, USA
[61a]INFN Sezione di Roma, I-00185 Roma, Italy
[61b]Dipartimento di Fisica, Università di Roma La Sapienza, I-00185 Roma, Italy
[62]Universität Rostock, D-18051 Rostock, Germany
[63]Rutherford Appleton Laboratory, Chilton, Didcot, Oxon, OX11 0QX, United Kingdom
[64]CEA, Irfu, SPP, Centre de Saclay, F-91191 Gif-sur-Yvette, France
[65]SLAC National Accelerator Laboratory, Stanford, California 94309 USA
[66]University of South Carolina, Columbia, South Carolina 29208, USA
[67]Stanford University, Stanford, California 94305-4060, USA
[68]State University of New York, Albany, New York 12222, USA
[69]Tel Aviv University, School of Physics and Astronomy, Tel Aviv, 69978, Israel
[70]University of Tennessee, Knoxville, Tennessee 37996, USA
[71]University of Texas at Austin, Austin, Texas 78712, USA
[72]University of Texas at Dallas, Richardson, Texas 75083, USA
[73a]INFN Sezione di Torino, I-10125 Torino, Italy
[73b]Dipartimento di Fisica Sperimentale, Università di Torino, I-10125 Torino, Italy
[74a]INFN Sezione di Trieste, I-34127 Trieste, Italy

[*]Deceased.
[†]Now at Temple University, Philadelphia, Pennsylvania 19122, USA.
[‡]Also with Università di Perugia, Dipartimento di Fisica, Perugia, Italy.
[§]Also with Università di Roma La Sapienza, I-00185 Roma, Italy.
[‖]Now at University of South Alabama, Mobile, Alabama 36688, USA.
[¶]Also with Laboratoire de Physique Nucléaire et de Hautes Energies, IN2P3/CNRS, Université Pierre et Marie Curie-Paris6, Université Denis Diderot-Paris7, F-75252 Paris, France.
[**]Also with Università di Sassari, Sassari, Italy.

[74b]*Dipartimento di Fisica, Università di Trieste, I-34127 Trieste, Italy*
[75]*IFIC, Universitat de Valencia-CSIC, E-46071 Valencia, Spain*
[76]*University of Victoria, Victoria, British Columbia, Canada V8W 3P6*
[77]*Department of Physics, University of Warwick, Coventry CV4 7AL, United Kingdom*
[78]*University of Wisconsin, Madison, Wisconsin 53706, USA*
(Received 30 April 2009; published 19 June 2009)

We present a measurement of the $B^0 \to \bar{\Lambda} p \pi^-$ branching fraction performed using the *BABAR* detector at the PEP-II asymmetric e^+e^- collider. Based on a sample of 467×10^6 $B\bar{B}$ pairs we measure $\mathcal{B}(B^0 \to \bar{\Lambda} p \pi^-) = [3.07 \pm 0.31\,(\text{stat}) \pm 0.23\,(\text{syst})] \times 10^{-6}$. The measured differential spectrum as a function of the dibaryon invariant mass $m(\bar{\Lambda} p)$ shows a near-threshold enhancement similar to that observed in other baryonic B decays. We study the $\bar{\Lambda}$ polarization as a function of $\bar{\Lambda}$ energy in the B^0 rest frame ($E^*_{\bar{\Lambda}}$) and compare it with theoretical expectations of fully longitudinally right-polarized $\bar{\Lambda}$ at large $E^*_{\bar{\Lambda}}$.

DOI: 10.1103/PhysRevD.79.112009 PACS numbers: 13.25.Hw, 13.60.Rj

I. INTRODUCTION

Observations of charmless three-body baryonic B decays have been reported recently by both the Belle and *BABAR* collaborations [1–3]. A common feature of these decay modes is the peaking of the baryon-antibaryon mass spectrum near threshold. This feature has stimulated considerable interest among theorists as a key element in the explanation of the unexpectedly high branching fractions for these decays [4,5].

In the standard model, the $B^0 \to \bar{\Lambda} p \pi^-$ decay proceeds through tree level $b \to u$ and penguin $b \to s$ amplitudes. It is of interest to study the structure of the decay amplitude in the Dalitz plane to test theoretical expectations. The weak decay $\bar{\Lambda} \to \bar{p}\pi^+$ is spin self-analyzing. Since the $\bar{s}$ quark carries the $\bar{\Lambda}$ spin, the V-A transition $b \to s$ leads to the expectation that the $\bar{\Lambda}$ is fully longitudinally right-polarized at large $\bar{\Lambda}$ energy in the B^0 rest frame [6]. This channel may also be used to search for direct CP violation.

II. DATA SET AND SELECTION

The data sample consists of 467×10^6 $B\bar{B}$ pairs, corresponding to an integrated luminosity of 426 fb^{-1}, collected at the $\Upsilon(4S)$ resonance with the *BABAR* detector. The detector is described in detail elsewhere [7]. Charged-particle trajectories are measured in a tracking system consisting of a five-layer double-sided silicon vertex tracker (SVT) and a 40-layer central drift chamber (DCH), both operating in a 1.5-T axial magnetic field. A ring-imaging Cherenkov detector (DIRC) is used for charged-particle identification. A CsI(Tl) electromagnetic calorimeter (EMC) is used to detect and identify photons and electrons, while muons and hadrons are identified in the instrumented flux return of the magnet (IFR). A *BABAR* detector Monte Carlo simulation based on GEANT4 [8] is used to optimize selection criteria and determine selection efficiencies.

We reconstruct $\bar{\Lambda}$ candidates in the $\bar{\Lambda} \to \bar{p}\pi$ decay mode as combinations of oppositely charged tracks, assign the proton and pion mass hypotheses, and fit to a common vertex [9]. Combinations with invariant mass in the range 1.111–1.121 GeV/c^2 are refit requiring the track pairs to originate from a common vertex and constraining the mass to the world-average Λ mass [10]. Candidate B^0 mesons are formed by combining $\bar{\Lambda}$ candidates with two additional oppositely charged tracks, each with momentum transverse to the beam greater than 50 MeV/c.

Measurements of the average energy loss (dE/dx) in the tracking devices, the angle of the Cherenkov cone in the DIRC, and energies deposited in the EMC and IFR are combined to give a likelihood estimator L_α for a track to be consistent with a given particle hypothesis α. We require that the Λ-decay proton candidates satisfy the particle-identification criteria $L_p/L_K > 0.33$ and $L_p/L_\pi > 1$ to discriminate from kaons and pions, respectively. The candidate protons, which are assumed to originate from the B^0 decay vertex, are analyzed with a selection algorithm based on bagged decision trees [11] which provide efficient particle discrimination, retaining 96.4% of the signal candidates and 17.8% of the background. The candidate pions from the B^0 vertex are required to pass a similar selection algorithm, tuned to discriminate pions, that retains 98.8% of the signal and 66.8% of the background. A Kalman fit [12] to the full decay sequence is used to reconstruct the B^0 vertex using the position of the beam spot and the total beam energy as kinematic constraints. Only candidates with a fit probability $P_{\text{vtx}} > 10^{-6}$ are considered, a requirement that retains 94.4% of the signal and 58.2% of the background.

The primary background arises from light-quark continuum events $e^+e^- \to q\bar{q}$ ($q = u, d, s, c$), which are characterized by collimation of final-state particles with respect to the quark direction, in contrast to the more spherical $B\bar{B}$ events. Exploiting this shape difference, we increase the signal significance using event-shape variables computed from the center-of-mass (CM) momenta of charged and neutral particles in the event. For each event, we combine the sphericity [13], the angle between the B^0 thrust axis and detector longitudinal axis, and the zeroth and second-order Legendre polynomial moments [14] of the tracks not asso-

ciated with the reconstructed B candidate, into a Fisher discriminant [15], where the coefficients are chosen to optimize the separation between signal and continuum-background Monte Carlo samples. We find that the selection using the optimal cut on the Fisher discriminant retains 72% of the candidates from the signal Monte Carlo sample and 8% from the continuum-background Monte Carlo sample.

To further reduce the combinatoric background, we take advantage of the long mean lifetime of Λ particles and require that the separation of the Λ and B^0 vertices, divided by its measurement error, computed on a per-candidate basis by the fit procedure, exceeds 20. This criterion is optimized on Monte Carlo events and is effective in rejecting 42% of combinatoric background that survives all other selection requirements, while retaining 90% of the signal candidates. The only sizable B^0 background is from the process $B^0 \to \bar{\Lambda}_c^- p \to \bar{\Lambda} p \pi^-$, which we suppress by removing candidates with an invariant mass $m(\bar{\Lambda}\pi^-)$ within 5 standard deviations (20 MeV/c^2) of the nominal Λ_c mass [10].

The kinematic constraints on B^0 mesons produced at the $\Upsilon(4S)$ allow further background discrimination from the variables $m_{\rm ES}$ and ΔE. We define $m_{\rm ES} = \sqrt{(\frac{s}{2} + \vec{p}_i \cdot \vec{p}_B)^2/E_i^2 - \vec{p}_B^2}$, where $(E_i, \vec{p}_i)$ is the four momentum of the initial e^+e^- system and $\vec{p}_B$ is the momentum of the reconstructed B^0 candidate, both measured in the laboratory frame, and s is the square of the total energy in the e^+e^- center-of-mass frame. We define $\Delta E = E_B^* - \frac{\sqrt{s}}{2}$, where E_B^* is the B^0 energy in the e^+e^- center-of-mass frame. Signal candidates have $m_{\rm ES}$ close to the B^0 mass and ΔE near zero. Candidates satisfying $|\Delta E| < 100$ MeV and $5.20 < m_{\rm ES} < 5.29$ GeV/c^2 are used in the maximum-likelihood fitting process.

III. BRANCHING FRACTION

We measure the branching fraction with a maximum-likelihood fit on the $m_{\rm ES}$-ΔE observables of reconstructed B^0 candidates. The ${}_s\mathcal{P}$lot technique [16] is then used to determine the $m(\bar{\Lambda}p)$ distribution and, after correcting for the nonuniform reconstruction efficiency, measure the $m(\bar{\Lambda}p)$-dependent differential branching fraction.

We consider as signal candidates only reconstructed B^0 candidates in which all particles are correctly assigned in the decay chain. By self-cross-feed, we refer to events in which B^0 mesons decay to $\bar{\Lambda}p\pi$ and are reconstructed as signal candidates in which one or more particles are not correctly assigned in the decay chain. An example of such a misreconstruction is where the protons from the signal B^0 and Λ decays are interchanged. We define the probability density function (PDF) in the ΔE-$m_{\rm ES}$ plane as the sum of signal, self-cross-feed, and background components. The likelihood function is given by

$$\mathcal{L} = \frac{1}{N!} e^{-(N_S + N_{\rm scf} + N_B)} \prod_{e=1}^{N} \{N_S \mathcal{P}_S(y_e) + N_{\rm scf} \mathcal{P}_{\rm scf}(y_e) + N_B \mathcal{P}_B(y_e)\}, \quad (1)$$

where $y_e = (m_{{\rm ES},e}, \Delta E_e)$, the product is over the N fitted candidates with N_S and N_B representing the numbers of signal and background events, and $N_{\rm scf} \equiv N_S f_{\rm scf}$ representing the self-cross-feed contribution. The three $\mathcal{P}$ functions are taken as products of one-dimensional ΔE and $m_{\rm ES}$ PDFs. We are justified in this simplification by the small correlation between these two variables in our Monte Carlo sample. The $m_{\rm ES}$ PDF is taken as a sum of two Gaussians for the signal and an ARGUS function [17] for the background. The ΔE PDF is taken as a sum of two Gaussians for the signal and a first-order polynomial for the background. Finally, the self-cross-feed contribution shows a peaking component that is modeled as the product of a sum of two Gaussians in ΔE, and a single Gaussian in $m_{\rm ES}$. We determine $f_{\rm scf} = 0.006$ and the other parameters that characterize this background from fits to simulated events.

We fit the means of the narrow ΔE and $m_{\rm ES}$ signal Gaussians, the coefficient in the exponential of the Argus function, the linear coefficient of the ΔE background distribution, and the event yields N_S and N_B. The means of the wide Gaussians are determined by applying Monte Carlo-determined offsets to the means of the narrow ones, such that only an overall shift of the fixed PDF shape is allowed. All other parameters used in the likelihood definition are fixed to values determined from fits to Monte Carlo-simulated events.

Once the maximum-likelihood fit provides the best estimates of the PDF parameters, we use the ${}_s\mathcal{P}$lot technique to reconstruct the efficiency-corrected $m(\bar{\Lambda}p)$ distribution and measure the branching fraction. The PDF is used to compute the s-weight for the nth component of event e as

$${}_s\mathcal{P}_n(y_e) = \frac{\sum_{j=1}^{n_c} \mathbf{V}_{nj} \mathcal{P}_j(y_e)}{\sum_{k=1}^{n_c} N_k \mathcal{P}_k(y_e)}, \quad (2)$$

where the indices n, j, and k run over the $n_c = 3$ signal, background, and self-cross-feed components. The symbol $\mathbf{V}_{nj}$ is the covariance matrix of the event yields as measured from the fit to the data sample. An important property of the ${}_s\mathcal{P}$lot is that the sum of the s-weights for the signal or background component equals the corresponding number of fitted signal or background events. We have demonstrated with simulated experiments that the ${}_s\mathcal{P}$lot is an unbiased and nearly optimal estimator of the $m(\bar{\Lambda}p)$ distribution. To retrieve the efficiency-corrected number of signal events in a given $m(\bar{\Lambda}p)$ bin J we use the s-weight sum

$$\tilde{N}_{S,J} = \sum_{e \in J} \frac{{}_s\mathcal{P}_S(y_e)}{\varepsilon(x_e)}, \quad (3)$$

where the per-event efficiency $\varepsilon(x_e)$ depends on the posi-

tion $x_e = (m_{\bar{\Lambda}p}, \cos\theta_{\bar{\Lambda}\pi})$ in the square Dalitz plane. Here $\theta_{\bar{\Lambda}\pi}$ is the angle between the momenta of the pion and the $\bar{\Lambda}$ candidate in the $\bar{\Lambda}p$ rest frame, and the efficiency is determined over a 20×20 grid in the Dalitz plane, using fully reconstructed signal-Monte Carlo events. The error $\sigma[\tilde{N}_{S,J}]$ in $\tilde{N}_{S,J}$ is given by

$$\sigma^2[\tilde{N}_{S,J}] = \sum_{e\in J}\left(\frac{{}_s\mathcal{P}_S(y_e)}{\varepsilon(x_e)}\right)^2. \quad (4)$$

An estimate of the efficiency-corrected number of signal events in the sample is given by the sum of the efficiency-corrected s-weights, or

$$\tilde{N}_S = \sum_J \tilde{N}_{S,J}, \quad (5)$$

and the branching fraction is obtained from

$$\mathcal{B}(B^0 \to \bar{\Lambda}p\pi^-) = \frac{\tilde{N}_S}{N_{B\bar{B}}\cdot\mathcal{B}(\Lambda \to p\pi)}, \quad (6)$$

where $N_{B\bar{B}}$ is the total number of $B\bar{B}$ pairs and $\mathcal{B}(\Lambda \to p\pi) = 0.639 \pm 0.005$ [10]. Using a collection of Monte Carlo pseudoexperiments, in which signal candidates, generated and reconstructed with a complete detector simulation, were mixed with background candidates, generated according to the background PDF, we confirm that this procedure provides a measurement of the branching fraction with negligible biases and accurate errors.

We can measure the CP-violating branching-fraction asymmetry by tagging the flavor of the B^0 ($\bar{B}^0$) meson with the charge of its daughter proton (antiproton). We repeat the maximum-likelihood fit described above including the partial rate asymmetry

$$\mathcal{A} = \frac{\mathcal{B}(\bar{B}^0 \to \Lambda\bar{p}\pi^+) - \mathcal{B}(B^0 \to \bar{\Lambda}p\pi^-)}{\mathcal{B}(\bar{B}^0 \to \Lambda\bar{p}\pi^+) + \mathcal{B}(B^0 \to \bar{\Lambda}p\pi^-)} \quad (7)$$

as a free parameter. We reduce the effect of systematic differences in particle-identification efficiencies between protons and antiprotons, and between positive and negative pions, by performing the fit on a sample of reconstructed candidates, where protons and pions that originate from the $\bar{\Lambda}$ decay satisfy the same particle-identification criteria as those imposed on the protons and pions that originate from the B^0 vertex.

IV. $\bar{\Lambda}$ POLARIZATION MEASUREMENT

We study the three orthogonal components of the polarization of $\bar{\Lambda}$ candidates reconstructed in the $B^0 \to \bar{\Lambda}p\pi^-$ decay as a function of $E^*_{\bar{\Lambda}}$, the $\bar{\Lambda}$ energy in the B^0 rest frame [6]. The distribution of the helicity angle $\theta_{\rm H}$ for the $\bar{\Lambda}$ decay is given by

$$\frac{1}{\Gamma}\frac{d\Gamma}{d\cos\theta_{\rm H}} = \frac{1}{2}[1 + \alpha_{\bar{\Lambda}}P(E^*_{\bar{\Lambda}})\cos\theta_{\rm H}], \quad (8)$$

where $\theta_{\rm H}$ is the angle between the antiproton direction, in the $\bar{\Lambda}$ rest frame, and either (1) $\hat{L}$, the unit vector in the direction of the $\bar{\Lambda}$ in the B^0 rest frame; (2) $\hat{T}$, the unit vector along the direction of the cross product between the momenta, in the B^0 rest frame, of the proton and the $\bar{\Lambda}$; or (3) $\hat{N} = \hat{L} \times \hat{T}$. The symbol $P(E^*_{\bar{\Lambda}})$ is the component of the $\bar{\Lambda}$ polarization in the $\hat{L}$, $\hat{T}$, or $\hat{N}$ direction as a function of $E^*_{\bar{\Lambda}}$, and $\alpha_{\bar{\Lambda}}$ is the $\bar{\Lambda}$ decay-asymmetry parameter [10]. CP conservation in $B^0 \to \bar{\Lambda}p\pi^-$ decays implies that

$$\alpha_\Lambda P_{[L,N],\bar{B}^0\to\Lambda\bar{p}\pi}(E^*_\Lambda) = \alpha_{\bar{\Lambda}}P_{[L,N],B^0\to\bar{\Lambda}p\pi}(E^*_{\bar{\Lambda}}), \quad (9)$$

while the product $\alpha_\Lambda P_T$ changes sign under CP conjugation. We use these relations to fit the B^0 and $\bar{B}^0$ candidate samples together.

We use a maximum-likelihood fit in $m_{\rm ES}$, ΔE, $E^*_{\bar{\Lambda}}$, and $\cos\theta_{\rm H}$ to measure the polarization as a function of $E^*_{\bar{\Lambda}}$ along each of the three axes defined above. We divide the $E^*_{\bar{\Lambda}}$ range into three bins with boundaries 1.10, 1.53, 1.80, and 2.40 GeV, chosen in order to have similar numbers of signal events in each bin. We define a PDF as the sum of signal and background components. The likelihood is

$$\mathcal{L} = \frac{1}{N!}\prod_{k=1}^{3} e^{-(N_{k,S}+N_{k,B})}\prod_{e=1}^{N_k}[N_{k,S}\mathcal{P}'_{k,S}(z_e)\mathcal{P}_S(y_e) + N_{k,B}\mathcal{P}'_{k,B}(z_e)\mathcal{P}_B(y_e)], \quad (10)$$

where we have divided the observables into two sets $y_e = (m_{\rm ES}, \Delta E)$ and $z_e = (\cos\theta_{\rm H}, E^*_{\bar{\Lambda}})$, and the products are over the three bins in $E^*_{\bar{\Lambda}}$ and over the N_k events that populate the kth bin, where $N_{k,S}$ and $N_{k,B}$ represent the numbers of fitted signal and background events. The $\mathcal{P}_{S,B}(y_e)$ PDFs are the same functions used in the branching-fraction measurement. However the self-cross-feed component is not included since it corresponds to a negligible fraction of the signal events. For the kth bin in $E^*_{\bar{\Lambda}}$, the signal ($\cos\theta_{\rm H}, E^*_{\bar{\Lambda}}$) PDF is written as the product of the differential branching fraction of Eq. (8), times the signal-reconstruction efficiency $\epsilon(\theta_{\rm H}, E^*_{\bar{\Lambda}})$:

$$\mathcal{P}'_{k,S}(\theta_{\rm H}, E^*_{\bar{\Lambda}}) = \tfrac{1}{2}\epsilon(\theta_{\rm H}, E^*_{\bar{\Lambda}})[1 + \{\alpha_{\bar{\Lambda}}P\}_k\cos\theta_{\rm H}], \quad (11)$$

where the $\{\alpha_{\bar{\Lambda}}P\}_k$ are fit parameters. The signal-selection efficiency is measured with a sample of reconstructed signal-Monte Carlo events that pass the same selection criteria as those used to define the data sample. We bin the signal efficiency in 20×20 rectangular boxes that cover the allowed region of the $E^*_{\bar{\Lambda}}$-$\cos\theta_{\rm H}$ plane (Fig. 1).

The background $\theta_{\rm H}$ distribution is modeled as a linear combination of Chebyshev polynomials up to fourth order. The four coefficients that define the linear combination are fitted independently for each of the three bins in $E^*_{\bar{\Lambda}}$. We study the $\theta_{\rm H}$ distribution of background events using candidates in the sideband region $m_{\rm ES} < 5.27$ GeV/c^2, and

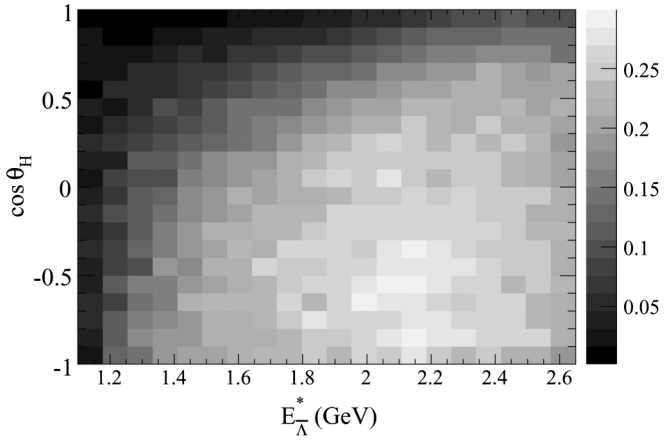

FIG. 1. Reconstruction efficiency measured on the Monte Carlo signal sample, as a function of $\cos\theta_{\rm H}$ and $E^*_{\bar{\Lambda}}$. In this plot $\theta_{\rm H}$ is the angle between the antiproton direction, in the $\bar{\Lambda}$ rest frame, and $\hat{L}$, the unit vector in the direction of the $\bar{\Lambda}$ in the B^0 rest frame.

find it to be nearly independent of $m_{\rm ES}$. We consider this insensitivity as an indication that the shape of the background $\theta_{\rm H}$ distribution is the same for events in and out of the signal region.

We have confirmed that this PDF representation does not bias the polarization measurement by performing pseudoexperiments in which signal candidates, generated and reconstructed with a complete detector simulation, were mixed with background candidates generated according to the observed helicity distribution in the $m_{\rm ES} < 5.27\ {\rm GeV}/c^2$ sideband. The number of signal and background candidates are chosen to match the characteristics of the data.

V. SYSTEMATIC UNCERTAINTIES

Systematic uncertainties in the branching-fraction measurement are listed in Table I and classified as overall uncertainties, uncertainties associated with event selection, and uncertainties associated with fitting the event distribution. We study the uncertainty due to tracking efficiency by comparing data and Monte Carlo for a sample of τ-pair events, in which one τ decays to one charged track and the other τ decays to three charged tracks. We separately study the tracking efficiency of Λ decay products using an inclusive sample of $\Lambda \to p\pi$ candidates and estimate an overall tracking reconstruction efficiency of 2.4%. The uncertainty associated with particle-identification (PID) selection criteria is estimated as 1.4% by comparing data and Monte Carlo identification efficiencies for protons from $\Lambda \to p\pi$ decays and pions from $K^0_S \to \pi\pi$ decays. The limited signal-Monte Carlo sample available to measure the reconstruction efficiency over the Dalitz plane results in an additional 0.4% contribution. The uncertainty in the number of $B\bar{B}$ pairs in the data sample accounts for a 1.1% contribution, while the assumption of a 50% ratio of $B^0\bar{B}^0$ to $B\bar{B}$ at the $\Upsilon(4S)$ gives an additional 3.2% contribution, computed from the difference between 50% and the current measured value $(48.4 \pm 0.6)\%$ [10].

Uncertainties associated with event-selection requirements on the Fisher discriminant and vertex fit probability are estimated by comparing data and Monte Carlo-selection efficiencies for a sample of $B^0 \to J/\psi K^0_S$ candidates. We use an inclusive sample of $\Lambda \to p\pi$ candidates to estimate uncertainties associated with the efficiencies of the flight-length significance and Λ-mass requirements.

The application of the requirement on the reconstructed $m(\Lambda\pi)$ invariant mass to suppress $B^0 \to \bar{\Lambda}_c p$ background

TABLE I. Systematic uncertainties on the branching-fraction measurement. ''Total'' is the sum in quadrature of all the individual contributions.

	Source	Uncertainty (%)
Overall	Tracking efficiency	2.4
	PID efficiency	1.4
	MC statistics	0.4
	$B\bar{B}$ counting	1.1
	$B^0\bar{B}^0/B\bar{B}$ fraction	3.2
	$\Lambda \to p\pi$ branching fraction	0.8
Event selection requirements	Event shape	1.0
	Fit probability	1.0
	Λ flight length	2.8
	Λ mass	2.4
	Λ_c veto	0.5
Fit procedure	Likelihood parameters	3.9
	ΔE resolution	1.7
	Self cross-feed fraction	0.8
	${}_s\mathcal{P}$lot bias	0.6
Total		7.4

has two associated systematic effects. The first results in an approximate 0.2% increase in the branching fraction due to the residual Λ_c component that survives the cut. The second results in an approximate 0.5% reduction of the branching fraction due to the reduced Dalitz-plot phase space. We correct for these effects and take the larger of the two as the uncertainty associated with the Λ_c veto cut.

We vary parameters that are kept fixed in the likelihood fit by their uncertainties, as measured on the signal-Monte Carlo sample fit, and measure the variation of the ${}_s\mathcal{P}$lot fitted result. The uncertainties associated with the parameters that enter the definition of the signal PDF are conservatively considered as correlated and are thus added to give a signal-PDF overall uncertainty of 3.2%, where the uncertainty in signal-$m_{\rm ES}$ fixed parameters accounts for a 1.9% contribution and that in signal-ΔE fixed parameters for a 1.3% contribution. The same procedure is applied to the parameters that enter the background PDF, with uncertainties determined on luminosity-weighted background-Monte Carlo samples, giving an additional 2.2% uncertainty. Finally, we combine the two uncertainties in quadrature and obtain a 3.9% uncertainty associated with the shapes of the signal and background models. The comparison of $B \to J/\psi K^0_S$ data and Monte Carlo samples reveals that the width of the ΔE Gaussian in the signal PDF can be underestimated in the Monte Carlo simulation by up to 5%, which translates to an additional 1.7% uncertainty.

We estimate possible biases associated with the determination of yields with the ${}_s\mathcal{P}$lot technique, using an ensemble of Monte Carlo experiments. Signal events, generated and reconstructed with a complete detector simulation, were mixed with background events, generated according to the background PDF. The numbers of events were chosen according to the expected yields in the data sample under study. We estimate an uncertainty of 0.6%.

The main systematic uncertainty in the polarization measurement is associated with the limited statistics of the Monte Carlo sample used to measure the signal-reconstruction efficiency in the $(\cos\theta_{\rm H}, E^*_{\bar\Lambda})$ plane, which results in $\alpha_{\bar\Lambda} P_L(E^*_{\bar\Lambda})$ uncertainties of 0.05, 0.07, and 0.04 for the three $E^*_{\bar\Lambda}$ bins. Variation of parameters fixed in the likelihood fit within their uncertainties provides additional contributions of 0.004, 0.03, and 0.03 in the three bins, respectively. We correct the fit result for the small biases we observe in a sample of Monte Carlo experiments, where background candidates were generated with the helicity distribution observed in $m_{\rm ES} < 5.27$ GeV$/c^2$ sideband data, and conservatively take these shifts as contributions to the systematic uncertainty.

VI. BRANCHING-FRACTION RESULTS

We select a total of 6360 candidates in the region $|\Delta E| < 100$ MeV, $m_{\rm ES} > 5.2$ GeV$/c^2$, $|m(\Lambda\pi) - m(\Lambda_c)| > 20$ MeV$/c^2$. Table II reports the fitted values of the two-dimensional $m_{\rm ES}$-ΔE PDF parameters, while

TABLE II. Branching-fraction results. N_S and N_B are the numbers of fitted signal and background events, respectively. The symbol $\mu(\Delta E)$ is the mean for the narrow Gaussian of the ΔE signal-PDF component, while $c_1(\Delta E)$ is the slope of the linear ΔE background PDF. $\mu(m_{\rm ES})$ is the mean for the Gaussian of the $m_{\rm ES}$ signal PDF, and $c_{\rm ARGUS}(m_{\rm ES})$ is the coefficient of the exponent in the background $m_{\rm ES}$ Argus function [17]. The uncertainties are statistical.

Parameter	Value
N_S	$183.3^{+19.2}_{-18.5}$
N_B	6176 ± 80
$\mu(\Delta E)$	-2.65 ± 1.84 MeV
$c_1(\Delta E)$	-3.5 ± 0.4 GeV^{-1}
$\mu(m_{\rm ES})$	5.2797 ± 0.0003 GeV$/c^2$
$c_{\rm ARGUS}(m_{\rm ES})$	-14.6 ± 1.45

Fig. 2 shows projections of the two-dimensional PDF on the $m_{\rm ES}$ and ΔE axes. Figure 3 shows the efficiency-corrected signal-${}_s\mathcal{P}$lot distribution of candidates as a function of $m(\bar\Lambda p)$, demonstrating a near-threshold enhancement similar to that observed in other baryonic B decays.

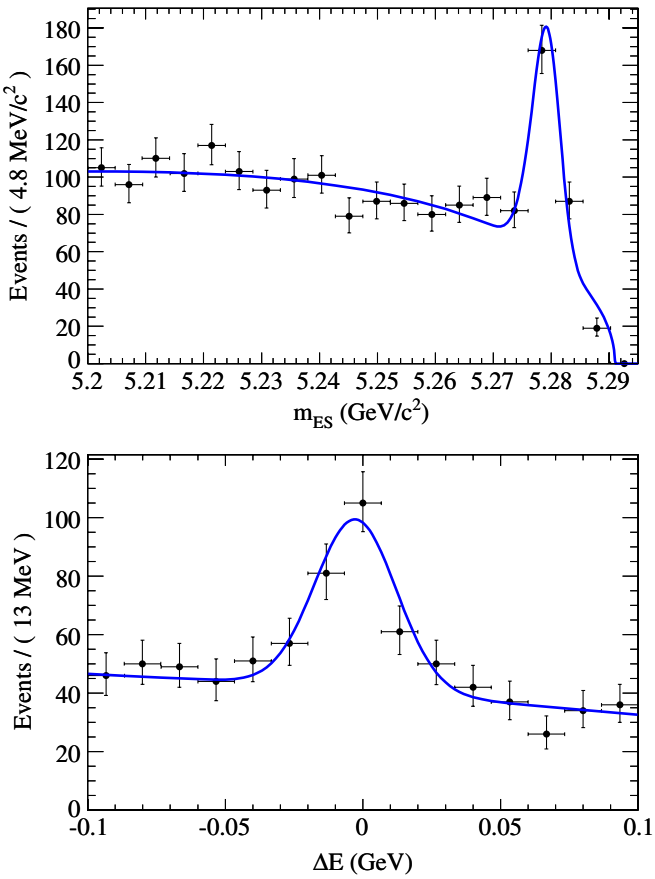

FIG. 2 (color online). Upper plot: $m_{\rm ES}$ distribution of candidates with $|\Delta E| < 27$ MeV. Lower plot: ΔE distribution of candidates with $m_{\rm ES} > 5.274$ GeV$/c^2$. The projections of the two-dimensional fit PDF are shown superimposed.

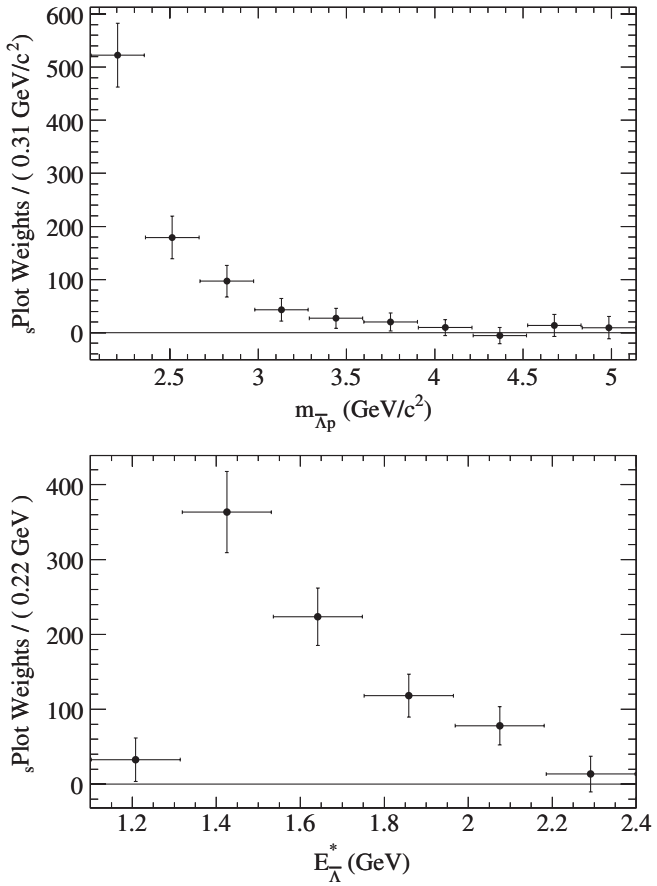

FIG. 3. Upper plot: $_s\mathcal{P}$lot of the $m(\bar{\Lambda}p)$ event distribution with efficiency corrections applied. Lower plot: $_s\mathcal{P}$lot of the $E^*_{\bar{\Lambda}}$ distribution with efficiency corrections applied. Horizontal bars represent bin ranges.

Summing the content of the efficiency-corrected $_s\mathcal{P}$lot bins, we obtain 916 ± 92 signal events, where the uncertainty is statistical. Using Eq. (6), we measure the branching fraction:

$$\mathcal{B}(B^0 \to \bar{\Lambda}p\pi^-) = [3.07 \pm 0.31\,(\text{stat}) \pm 0.23\,(\text{syst})] \times 10^{-6}.$$

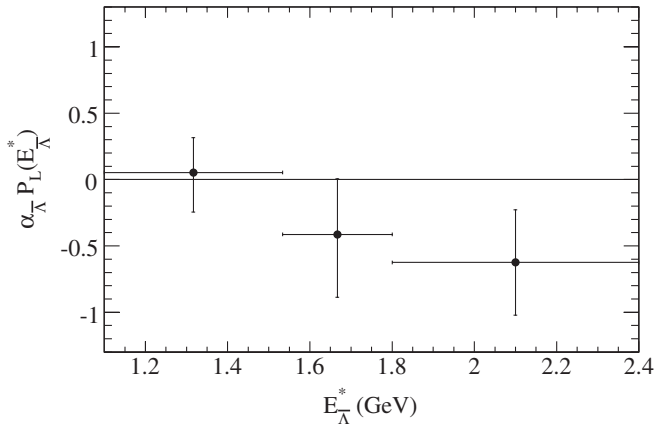

FIG. 4. The product of $\bar{\Lambda}$ longitudinal polarization and $\alpha_{\bar{\Lambda}}$ as a function of $E^*_{\bar{\Lambda}}$. Horizontal bars represent bin ranges.

This measurement, which is compatible with a previous measurement by the Belle collaboration [3], confirms the peaking of the baryon-antibaryon mass spectrum near threshold, a feature that plays a key role in the explanation of the larger branching fractions of three-body baryonic B decays compared to two-body decays [5]. From the maximum-likelihood fit to the branching-fraction asymmetry we obtain

$$\mathcal{A} = -0.10 \pm 0.10\,(\text{stat}) \pm 0.02\,(\text{syst}),$$

which is compatible with zero asymmetry.

VII. POLARIZATION RESULTS

Only 3994 candidates populate the $E^*_{\bar{\Lambda}}$ range [1.1, 2.4] GeV. Signal candidates are absent in the region with $E^*_{\bar{\Lambda}} > 2.4$ GeV (Fig. 3) as a kinematical consequence of the near-threshold peaking of the baryon-antibaryon mass spectrum.

We plot in Fig. 4 the values of the longitudinal polarization product $\alpha_{\bar{\Lambda}} P_L(E^*_{\bar{\Lambda}})$ obtained from the maximum-likelihood fit. Table III displays the longitudinal, transverse, and normal polarization measurements in each of the three $E^*_{\bar{\Lambda}}$ bins, assuming $\alpha_{\bar{\Lambda}} = -0.642 \pm 0.013$ for the

TABLE III. Polarization results. N_S and N_B are the numbers of fitted signal and background candidates in each $E^*_{\bar{\Lambda}}$ bin. We report the values of the longitudinal, transverse, and normal $\bar{\Lambda}$ polarizations in each of the three $E^*_{\bar{\Lambda}}$ bins.

$E^*_{\bar{\Lambda}}$ range (GeV)	1.10–1.53	1.53–1.80	1.80–2.40
N_S	63 ± 9	51 ± 9	55 ± 11
N_B	519 ± 23	643 ± 26	2663 ± 52
P_L	$-0.08^{+0.47}_{-0.40} \pm 0.09$	$+0.64^{+0.73}_{-0.65} \pm 0.12$	$+0.97^{+0.62}_{-0.62} \pm 0.08$
P_T	$+0.25^{+0.53}_{-0.58} \pm 0.09$	$+0.56^{+0.42}_{-0.48} \pm 0.12$	$+0.05^{+0.61}_{-0.60} \pm 0.08$
P_N	$-0.64^{+0.34}_{-0.33} \pm 0.09$	$-0.78^{+0.39}_{-0.36} \pm 0.12$	$+0.26^{+0.53}_{-0.53} \pm 0.08$

$\bar{\Lambda}$ decay-asymmetry parameter [10]. The results are consistent with full longitudinal right-polarization of $\bar{\Lambda}$'s from $B^0 \to \bar{\Lambda} p \pi^-$ decays at large $E^*_{\bar{\Lambda}}$ (Λ's would be oppositely polarized). The transverse polarization is not expected to be zero because of the presence of strong final-state interactions.

VIII. CONCLUSIONS

Based on 467×10^6 $B\bar{B}$ pairs collected by the *BABAR* detector at PEP-II, we present a measurement of the $B^0 \to \bar{\Lambda} p \pi^-$ branching fraction and confirm the peaking of the baryon-antibaryon mass spectrum near threshold, characteristic of three-body baryonic B decays. In addition we measure the $\bar{\Lambda}$ polarization in $B^0 \to \bar{\Lambda} p \pi^-$ decays as a function of $E^*_{\bar{\Lambda}}$. The measurement is compatible with the theoretical prediction of full longitudinal right-handed polarization for large $E^*_{\bar{\Lambda}}$, which follows from the purely left-handed $b \to s$ transition in the standard model [6].

ACKNOWLEDGMENTS

We are grateful for the extraordinary contributions of our PEP-II colleagues in achieving the excellent luminosity and machine conditions that have made this work possible. The success of this project also relies critically on the expertise and dedication of the computing organizations that support *BABAR*. The collaborating institutions wish to thank SLAC for its support and the kind hospitality extended to them. This work is supported by the U.S. Department of Energy and National Science Foundation, the Natural Sciences and Engineering Research Council (Canada), the Commissariat à l'Energie Atomique and Institut National de Physique Nucléaire et de Physique des Particules (France), the Bundesministerium für Bildung und Forschung and Deutsche Forschungsgemeinschaft (Germany), the Istituto Nazionale di Fisica Nucleare (Italy), the Foundation for Fundamental Research on Matter (The Netherlands), the Research Council of Norway, the Ministry of Education and Science of the Russian Federation, Ministerio de Educación y Ciencia (Spain), and the Science and Technology Facilities Council (United Kingdom). Individuals have received support from the Marie-Curie IEF program (European Union) and the A. P. Sloan Foundation.

[1] M. Z. Wang *et al.* (Belle Collaboration), Phys. Rev. Lett. **90**, 201802 (2003).
[2] B. Aubert *et al.* (*BABAR* Collaboration), Phys. Rev. D **72**, 051101 (2005).
[3] M. Z. Wang *et al.* (Belle Collaboration), Phys. Rev. D **76**, 052004 (2007). Based on a 414 fb^{-1} data sample, Belle reports the measurement of the branching fraction: $\mathcal{B}(B^0 \to \bar{\Lambda} p \pi^-) = [3.23^{+0.33}_{-0.29}\,(\text{stat}) \pm 0.29\,(\text{syst})] \times 10^{-6}$.
[4] W. S. Hou and A. Soni, Phys. Rev. Lett. **86**, 4247 (2001).
[5] C. K. Chua and W. S. Hou, Eur. Phys. J. C **29**, 27 (2003).
[6] M. Suzuki, J. Phys. G **29**, B15 (2003).
[7] B. Aubert *et al.* (*BABAR* Collaboration), Nucl. Instrum. Methods Phys. Res., Sect. A **479**, 1 (2002).
[8] S. Agostinelli *et al.*, Nucl. Instrum. Methods Phys. Res., Sect. A **506**, 250 (2003).
[9] Inclusion of the charge conjugate mode is implied.
[10] C. Amsler *et al.*, Phys. Lett. B **667**, 1 (2008).
[11] L. Breiman, Mach. Learn. **24**, 123 (1996).
[12] W. D. Hulsbergen, Nucl. Instrum. Methods Phys. Res., Sect. A **552**, 566 (2005).
[13] G. Hanson *et al.*, Phys. Rev. Lett. **35**, 1609 (1975).
[14] The zeroth and second-order Legendre polynomial moments are defined as follows: $L_0 = \sum_i p_i^*$ and $L_2 = \sum_i \frac{1}{2} p_i^* (3\cos^2\theta_i^* - 1)$, where p_i^* are the magnitudes of the momenta of the tracks and neutral clusters not associated with the reconstructed B^0 candidate and θ_i^* are the angles between the momenta and the B^0 thrust axis.
[15] R. A. Fisher, Annals of Eugenics **7**, 179 (1936).
[16] F. R. Le Diberder and M. Pivk, Nucl. Instrum. Methods Phys. Res., Sect. A **555**, 356 (2005).
[17] H. Albrecht *et al.* (ARGUS Collaboration), Z. Phys. C **48**, 543 (1990). The ARGUS function is defined as: $\text{Ar}(m; m_0, c) = B \frac{m}{m_0} (1 - \frac{m^2}{m_0^2})^{1/2} \exp[c(1 - \frac{m^2}{m_0^2})]$.